Representation of Electromagnetic Fields over Arbitrary Surfaces by a Finite and Nonredundant Number of Samples

Ovidio M. Bucci, *Fellow, IEEE*, Claudio Gennarelli, and Catello Savarese

***Abstract*— In this paper, it is shown that the electromagnetic (EM) field, radiated or scattered by bounded sources, can be accurately represented over a substantially arbitrary surface by a finite number of samples even when the observation domain is unbounded. The number of required samples is nonredundant and essentially coincident with the number of degrees of freedom of the field. This result relies on the extraction of a proper phase factor from the field expression and on the use of appropriate coordinates to parameterize the domain. It is demonstrated that the number of degrees of freedom is independent of the observation domain and depends only on the source geometry. The case of spheroidal sources and observation domains with rotational symmetry is analyzed in detail and the particular cases of spherical and planar sources are explicitly considered. For these geometries, precise and fast sampling algorithms of central type are presented, which allow an efficient recovery of EM fields from a nonredundant finite number of samples. Such algorithms are stable with respect to random errors affecting the data.**

***Index Terms*—Electromagnetic fields, sampling methods.**

I. Introduction

SAMPLING representations of radiated or scattered fields are usually more convenient and efficient than those based on modal or asymptotic expansions since the expansion coefficients are the field samples (i.e., directly available quantities) and the basis functions are simple and universal. Accordingly, they can be used on any observation surface.

Sampling techniques have long been applied to antenna problems, although heuristically and with great data redundancy, but only recently have they received a rigorous theoretical assessment. This was allowed by the demonstration [1] that electromagnetic (EM) fields radiated or scattered by finite sources, enclosed in a sphere of radius a, and observed on an analytical surface $\mathcal{M}$ external to it can be well approximated by spatially bandlimited functions, provided the phase propagation factor $\exp(-j\beta r)$, where β is the wavenumber and r the distance from the sphere center, is extracted from the field expression and a proper parameterization is used to describe $\mathcal{M}$. Indeed, for large scatterers ($\beta a \gg 1$), the band-limitation error exhibits a step-like behavior decreasing more than exponentially as the bandwidth exceeds a critical value, practically equal to βa. Accordingly, the "reduced" field $\mathbf{F}(\boldsymbol{r}) = \mathbf{E}(\boldsymbol{r}) \exp(j\beta r)$ can be described by functions bandlimited to $\chi'\beta a$ where χ' is a factor slightly greater than unity. Consequently, sampling interpolation techniques can be used to represent the field and can be applied to antenna pattern evaluation as well as to near-field far-field (NF-FF) transformation techniques. To this end, by taking advantage of the above properties, efficient sampling interpolation algorithms of central type have been developed for several geometries. These algorithms are optimal since they minimize the truncation error for a given number of retained samples and, as compared with the cardinal series expansions, are more stable with respect to errors affecting the data. Finally, starting from these expansions, accurate, computationally manageable, and stable sampling algorithms appropriate to nonuniform sample distributions over various surfaces have been proposed. A review of the more relevant results can be found in [2].

In the case of a spherical observation domain centered on the source, the number of required samples is finite regardless of the sphere size and coincides essentially with the number of degrees of freedom of the field [3], i.e., the number of independent parameters necessary to represent it with a given accuracy outside the smallest sphere enclosing the source. This "nonredundancy" is not shared by the available sampling representations over nonspherical surfaces. In the case of unbounded surfaces such as the plane and the cylinder, the number of required samples increases with the extension of the region wherein the field is significant, which can lead to a large redundancy. Moreover, the hypothesis that the source is contained in a sphere is not always the most natural one. For instance, for aperture-type antennas, this assumption does not make it possible to consider observation domains close to the antenna, which can be a relevant practical drawback and again leads to redundancies.

This paper aims to overcome the above drawbacks, obtaining efficient representations of EM fields, which require a finite and nonredundant number of samples, even when the source is not spherical and the observation domain is unbounded.

We stress that while in "direct" problems the redundancy of the representation affects the efficiency but not the stability of the algorithms, the situation is completely different when dealing with "inverse" problems such as inverse scattering,

Manuscript received August 3, 1995; revised November 11, 1997. This work was supported in part by the Italian Ministry of University and Scientific Research.

O. M. Bucci is with the Dipartimento di Ingegneria Elettronica, Universitá "Federico II," Napoli, 80125 Italy.

C. Gennarelli is with the Dipartimento di Ingegneria dell'Informazione e Ingegneria Elettrica, Universitá di Salerno, Fisciano (Salerno), 84084 Italy.

C. Savarese is with the Istituto di Teoria e Tecnica delle Onde Elettromagnetiche, Istituto Universitario Navale, Napoli, 80133 Italy.

Publisher Item Identifier S 0018-926X(98)02264-9.

phase retrieval, image restoration, and antenna synthesis. In fact, the ill-posedness of these problems makes it impossible to recover, from unavoidably inaccurate data, a number of independent parameters larger than the number of degrees of freedom of the field [4].

In Section II, with explicit reference to the source and the observation domain geometry, the approach developed in [1] is generalized to establish the proper phase factor to be extracted from the field expression and the appropriate parameterization of the observation surface. Furthermore, the number of degrees of freedom is established for sources enclosed in a convex domain with rotational symmetry and a "natural" coordinate system is introduced to describe the field. In Section III, the case of spheroidal sources is considered in detail together with the particular cases of spherical and planar sources. Interpolation formulas of central type are established in Section IV, wherein numerical examples of recovery of radiated fields from nonredundant samples are also shown. Some conclusions are collected in Section V.

II. Optimal Parameterization and Degrees of Freedom of EM Fields

Since any observation surface $\mathcal{M}$ can be described by two families of coordinate curves, let us consider first the electric field radiated by an arbitrary finite source over an analytical curve $\mathcal{C}$. In the frequency domain and $\exp(j\omega t)$ convention, we have (Fig. 1)

$$\mathbf{E}(\boldsymbol{r}) = -\frac{j\beta\zeta}{4\pi}\int_V \left[\underline{\underline{I}} + \frac{\nabla\nabla}{\beta^2}\right]\frac{\exp(-j\beta R)}{R} \cdot \boldsymbol{J}(\boldsymbol{r}')\,d\boldsymbol{r}' = \int_V \underline{\underline{G}}_0(\boldsymbol{r},\boldsymbol{r}')\cdot\boldsymbol{J}(\boldsymbol{r}')\,d\boldsymbol{r}' \tag{1}$$

where $\underline{\underline{I}}$ is the identity matrix, $\boldsymbol{J}(\boldsymbol{r}')$ is the (true or equivalent) source current density, ζ is the free-space impedance, $\underline{\underline{G}}_0$ is the dyadic Green function, $R = |\boldsymbol{r} - \boldsymbol{r}'|$, and V is the volume occupied by the source.

Let us now define the "generalized reduced field" over $\mathcal{C}$ as

$$\mathbf{F}(\xi) = \mathbf{E}(\xi)\exp[j\psi(\xi)] \tag{2}$$

where $\boldsymbol{r} = \boldsymbol{r}(\xi)$ is an arbitrary parameterization of the curve and ψ is a phase function (both analytical) to be determined. Accordingly

$$\mathbf{F}(\xi) = -\frac{j\beta\zeta}{4\pi}\int_V \frac{\exp(j\gamma)}{R} \cdot\left[\underline{\underline{I}} + R\exp(j\beta R)\frac{\nabla\nabla}{\beta^2}\frac{\exp(-j\beta R)}{R}\right] \cdot \boldsymbol{J}(\boldsymbol{r}')\,d\boldsymbol{r}' = \int_V \underline{\underline{G}}(\boldsymbol{r}(\xi),\boldsymbol{r}')\cdot\underline{\mathbf{J}}(\boldsymbol{r}')\,d\boldsymbol{r}' \tag{3}$$

where

$$\gamma(\xi,\boldsymbol{r}') = \psi(\xi) - \beta R(\xi,\boldsymbol{r}'). \tag{4}$$

The best approximation (in mean-square norm) of $\mathbf{F}$ with a function bandlimited to w is[1]

$$\mathbf{F}_w = \frac{1}{\pi}\frac{\sin w\xi}{\xi} * \mathbf{F}(\xi) \tag{5}$$

[1]The Dirichlet kernel should be used in the case of closed curves.

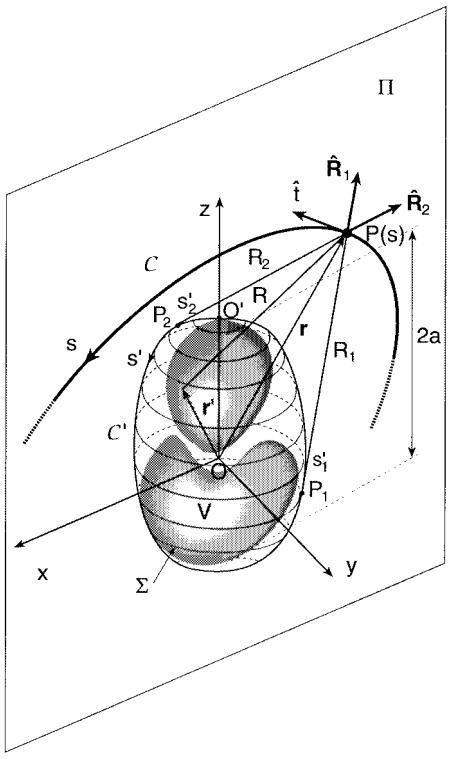

Fig. 1. Geometry of the problem.

where the asterisk stands for convolution. The corresponding error is

$$\Delta\mathbf{F}(\xi) = \mathbf{F}_w(\xi) - \mathbf{F}(\xi) = \int_V [\underline{\underline{G}}_w(\xi,\boldsymbol{r}') - \underline{\underline{G}}(\xi,\boldsymbol{r}')] \cdot \boldsymbol{J}(\boldsymbol{r}')\,d\boldsymbol{r} = \int_V \Delta\underline{\underline{G}}(\xi,\boldsymbol{r}')\cdot\boldsymbol{J}(\boldsymbol{r}')\,d\boldsymbol{r}' \tag{6}$$

whose modulus is sharply bounded as follows:

$$|\Delta\mathbf{F}(\xi)| \le \max_{\boldsymbol{r}'\in V,\xi} |\Delta\underline{\underline{G}}(\xi,\boldsymbol{r}'|\int_V |\underline{\mathbf{J}}(\boldsymbol{r}')|\,d\boldsymbol{r}'. \tag{7}$$

$\Delta\underline{\underline{G}}$ can be asymptotically evaluated by the steepest descent method in a way similar to that exploited in [1]. The stationary points are given by the condition

$$\pm w + \frac{\partial}{\partial\xi}\gamma(\xi,\boldsymbol{r}') = \pm w + \frac{\partial}{\partial\xi}[\psi(\xi) - \beta R(\xi,\boldsymbol{r}')] = 0. \tag{8}$$

By paralleling the reasoning in [1], it turns out that for large sources and observation domains not too near V, the band-limitation error (7) exhibits a step-like behavior and becomes vanishingly small as the bandwidth w exceeds the critical value

$$W = \max_{\boldsymbol{r}',\xi}\left|\frac{\partial\gamma}{\partial\xi}\right| = \max_{\xi}\left[\max_{\boldsymbol{r}'}\left|\frac{\partial\gamma}{\partial\xi}\right|\right] = \max_{\xi}\ w(\xi). \tag{9}$$

This value is naturally identified as the effective bandwidth corresponding to the chosen parameterization $\boldsymbol{r} = \boldsymbol{r}(\xi)$ and phase function $\psi = \psi(\xi)$. Now, for a given curve parameterization, it is clear that to obtain a nonredundant representation, we must choose the phase factor in such a way as to minimize for any ξ the "local" bandwidth $w(\xi)$. From (4) and (9), we find that this is accomplished by making the derivative of

ψ equal to the average between the maximum and minimum values of $\beta\partial R/\partial\xi$ when $\boldsymbol{r}'$ assumes all the positions in V, i.e.,

$$\frac{d\psi(\xi)}{d\xi} = \frac{\beta}{2}\left[\max_{\boldsymbol{r}'}\frac{\partial R}{\partial s} + \min_{\boldsymbol{r}'}\frac{\partial R}{\partial s}\right]\frac{ds}{d\xi} = \frac{\beta}{2}[\max_{\boldsymbol{r}'}\hat{\boldsymbol{R}}\cdot\hat{\boldsymbol{t}} + \min_{\boldsymbol{r}'}\hat{\boldsymbol{R}}\cdot\hat{\boldsymbol{t}}]\frac{ds}{d\xi} \quad (10)$$

where s is the arclength, $\hat{\boldsymbol{t}}$ is the unit-vector tangent to $\mathcal{C}$ at $P(\xi)$, and $\hat{\boldsymbol{R}}$ is the unit vector pointing from $\boldsymbol{r}'$ to P (Fig. 1). Therefore, the required phase factor to be singled out is

$$\psi(\xi) = \int d\psi(\xi) = \frac{\beta}{2}\int_0^{s(\xi)}\left[\max_{\boldsymbol{r}'}\frac{\partial R}{\partial s} + \min_{\boldsymbol{r}'}\frac{\partial R}{\partial s}\right]ds + \text{const.} \quad (11)$$

Once ψ has been chosen according to (11), by taking (4) and (9) into account we get

$$w(\xi) = \frac{\beta}{2}\left[\max_{\boldsymbol{r}'}\frac{\partial R}{\partial s} - \min_{\boldsymbol{r}'}\frac{\partial R}{\partial s}\right]\frac{ds}{d\xi} = \frac{\beta}{2}[\max_{\boldsymbol{r}'}\hat{\boldsymbol{R}}\cdot\hat{\boldsymbol{t}} - \min_{\boldsymbol{r}'}\hat{\boldsymbol{R}}\cdot\hat{\boldsymbol{t}}]\frac{ds}{d\xi}. \quad (12)$$

Let us now consider the optimal choice of the parameter ξ. The choice made in [1], i.e., a normalized arclength generally causes the local bandwidth w to be variable with ξ. As a consequence, the sample spacing, which is dictated by the bandwidth W, becomes unnecessarily small in the zones, wherein $w(\xi)$ is smaller than its maximum value. This obviously leads to redundancy in the corresponding sampling representations. This suggests determining ξ by ensuring that the local bandwidth $w(\xi)$ is constant and equal to W. Accordingly

$$\xi = \xi(s) = \frac{\beta}{2W}\int_0^S\left[\max_{\boldsymbol{r}'}\frac{\partial R}{\partial s} - \min_{\boldsymbol{r}'}\frac{\partial R}{\partial s}\right]ds. \quad (13)$$

Note that a change of W is reflected in a simple change of scale in the parameterization and vice versa. Expressions (11) and (13) give the optimal phase factor and parameterization.

In order to take the source geometry into account in a realistic and flexible way, let us consider (instead of a sphere) the smallest convex domain $\mathcal{B}$ with rotational symmetry, enclosing V, and denote by Σ its surface and $2a$ its diameter (Fig. 1).

With reference to an observation curve lying on a meridian plane Π, let us denote with $\mathcal{C}'$ the intersection between Π and Σ. Due to the involved symmetry, it is clear that the extreme values of the quantity $\partial R/\partial s = \hat{\boldsymbol{R}}\cdot\hat{\boldsymbol{t}}$ in (11) and (13) occur at the two tangency points $P_{1,2}$[2] (Fig. 1). Denoting by $s'_{1,2}$ the arclength coordinates of the points $P_{1,2}$, we have

$$R_{1,2} = |\boldsymbol{r}(s) - \boldsymbol{r}'(s'_{1,2})| = R(s, s'_{1,2}) = R[s, s'_{1,2}(s)] \quad (14)$$

hence

$$\frac{dR_{1,2}}{ds} = \left.\frac{\partial R}{\partial s}\right|_{s'_{1,2}} + \frac{\partial R}{\partial s'_{1,2}}\,\frac{ds'_{1,2}}{ds} = \left.\frac{\partial R}{\partial s}\right|_{s'_{1,2}} \mp \frac{ds'_{1,2}}{ds} \quad (15)$$

[2]It is assumed that $\hat{\boldsymbol{t}}$ is external to the cone of vertex P tangent to Σ.

because $\partial R/\partial s'_{1,2} = \mp 1$, being $P_{1,2}$ tangency points. Accordingly

$$\left.\frac{\partial R}{\partial s}\right|_{s'_{1,2}} = \frac{dR_{1,2}}{ds} \pm \frac{ds'_{1,2}}{ds} = \frac{d(R_{1,2} \pm s'_{1,2})}{ds}. \quad (16)$$

Taking (11) and (13) into account, we immediately get

$$\psi = \beta\left[\frac{R_1 + R_2}{2} + \frac{s'_1 - s'_2}{2}\right] + \text{const} \quad (17)$$

$$\xi = \frac{\beta}{W}\left[\frac{R_1 - R_2}{2} + \frac{s'_1 + s'_2}{2}\right] + \text{const.} \quad (18)$$

Relations (17) and (18) reduce the evaluation of ψ and ξ to that of quantities having a simple geometrical meaning. They show that ψ and ξ at the point P depend only on the point itself and not on the considered curve through it. Hence, the couple (ψ, ξ) provides a coordinate system for the points (external to Σ) on any meridian plane. This "natural" coordinate system is orthogonal and from relations (15)–(18) we get

$$\frac{d\psi}{ds} = \beta\frac{\partial}{\partial s}\left(\frac{R_1 + R_2}{2}\right) = \beta\left(\frac{\hat{\boldsymbol{R}}_1 + \hat{\boldsymbol{R}}_2}{2}\right)\cdot\hat{\boldsymbol{t}}$$

$$\frac{d\xi}{ds} = \frac{\beta}{W}\,\frac{\partial}{\partial s}\left(\frac{R_1 - R_2}{2}\right) = \frac{\beta}{W}\left(\frac{\hat{\boldsymbol{R}}_1 - \hat{\boldsymbol{R}}_2}{2}\right)\cdot\hat{\mathbf{t}}. \quad (19)$$

Accordingly, the coordinate curves through P are perpendicular to $\hat{\boldsymbol{R}}_1 + \hat{\boldsymbol{R}}_2$ and $\hat{\boldsymbol{R}}_1 - \hat{\boldsymbol{R}}_2$, respectively, and, hence, orthogonal. Putting the constants in (17) and (18) equal to zero, the curve $\psi = 0$ coincides with $\mathcal{C}'$ and the coordinate curve $\xi = 0$ intersects $\mathcal{C}'$ at $s' = 0$. As P goes to infinity, we have $\psi \sim \beta r$ so that ψ is a (normalized) radial-like coordinate. On the other hand, ξ is an angle-like coordinate whose variation when P encircles the source once equals $\beta\ell'/W$, ℓ' being the length of $\mathcal{C}'$. This suggests choosing $W = \beta\ell'/2\pi$ so that ξ covers a 2π range.

The above property implies that the number of points at Nyquist spacing $\Delta\xi = \pi/W$ lying on *any* meridian closed curve encircling $\mathcal{C}'$ is *finite, constant* and equal to

$$N_\xi = \frac{\beta\ell' W}{W\pi} = \frac{2\ell'}{\lambda}. \quad (20)$$

Accordingly, the field over such a curve can be represented with a sampling expansion using a number of samples n slightly larger than N_ξ. By paralleling the reasoning of [3], it turns out that the corresponding error goes to zero exponentially with $n - N_\xi$ provided that γ and ξ are indeed analytical over $\mathcal{C}$, i.e., if (and only if) both $\mathcal{C}$ and $\mathcal{C}'$ are analytical closed curves. The same conclusions also hold if we are interested in representing the field only on a segment of $\mathcal{C}$ provided that some few guard samples outside the interval of interest are retained or more sophisticated representations involving spheroidal functions are adopted [3]. When the hypothesis on $\mathcal{C}$ and $\mathcal{C}'$ are not satisfied, the asymptotic behavior is dominated by the nonregular points of $\gamma(\xi)$ and the error decreases only algebraically. Accordingly, sampling representations can still be used but the bandlimitation error can assume larger values in the neighborhood of those points of the observation curve wherein γ or ξ (or both) are not regular.

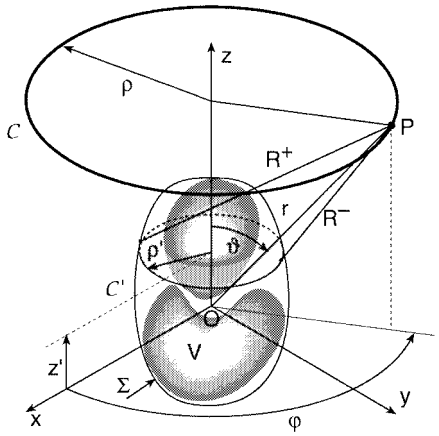

Fig. 2. Geometry relevant to an azimuthal observation circumference.

Let us now turn to consider an azimuthal circle (see Fig. 2). Due to the symmetry, the extreme values of $\partial R/\partial s$ are opposite and constant along the circle. It thus follows from (11) and (13) that the phase function is constant and that any parameter proportional to the arclength is optimal. It is convenient to choose for the phase function the value of ψ corresponding to the considered circle in the previously introduced meridian coordinate system (ψ, ξ) and to choose the azimuthal angle φ as parameter. In this way, the triple (ψ, ξ, φ) constitutes an orthogonal coordinate system in the space outside the surface Σ enclosing the source. Appendix A shows that the bandwidth relevant to a circle of radius ρ and center $(0, 0, z)$ is given by

$$\begin{aligned} W_\varphi = W_\varphi(\rho, z) &= \frac{\beta}{2} \max_{z'}(R^+ - R^-) \\ &= \frac{\beta}{2} \max_{z'}(\sqrt{(z-z')^2 + (\rho + \rho'(z))^2} \\ &\quad - \sqrt{(z-z')^2 + (\rho - \rho'(z'))^2}) \end{aligned} \tag{21}$$

wherein $\rho'(z')$ is the equation of Σ in cylindrical coordinates. It is worth noting that, as can be shown by simple geometrical reasonings, the maximum is attained on that zone of surface lying on the same side of the observation circle with respect to its maximum transverse circle.

It can be easily shown that the following sharp bound holds for W_φ:

$$W_\varphi \leq \beta \rho'_{\max} \tag{22}$$

$\rho'_{\max}$ being the maximum transverse radius of Σ.

As the circle moves toward infinity, we have

$$W_\varphi \underset{\rho^2 + z^2 \to \infty}{\sim} \beta \rho'_{\max} \frac{\rho}{\sqrt{\rho^2 + z^2}} = \beta \rho'_{\max} \sin \vartheta \tag{23}$$

ϑ being the polar angle of the circle points. On the other hand, as the circle shrinks to Σ, direct application of the triangular inequality to (21) gives

$$W_\varphi \underset{\rho \to \rho'(z)}{\sim} \beta \rho'(z). \tag{24}$$

According to the above results, by applying sampling expansion along φ and ξ, we can represent the field over any observation surface (with the same rotational symmetry as the source) in terms of a *finite* number of samples.

For large sources, we can choose a surface $\tilde{\Sigma}$ that is simultaneously sufficiently far from Σ (in terms of wavelengths) for asymptotic analysis to apply, yet sufficiently near to it (in terms of source diameter $2a$) to make the estimate (24) for W_φ valid. For such a surface, the overall number N of samples at Nyquist rate is given by

$$\begin{aligned} N &= \sum_{i=1}^{N_\xi/2} \frac{2\pi}{\pi/W_\varphi(\xi_i)} \cong \frac{\beta}{\pi} \frac{W}{\pi} \sum_{i=1}^{N_\xi/2} 2\pi \tilde{\rho}(\xi_i) \Delta\xi \\ &\cong \frac{\beta}{\pi} \frac{W}{\pi} \int_0^{2\pi} d\varphi \int_0^{\beta \ell'/2W} \tilde{\rho}(\xi)\, d\xi \\ &\cong \frac{\beta}{\pi} \frac{W}{\pi} \int_0^{2\pi} d\varphi \int_0^{\beta \ell'/2W} \rho'(\xi)\, d\xi \end{aligned} \tag{25}$$

wherein $\tilde{\rho}(\xi)$ and $\rho'(\xi)$ denote the transverse radius of $\tilde{\Sigma}$ and Σ, respectively. Taking (18) into account, we get from (25)

$$N \cong \frac{\beta^2}{\pi^2} \int_0^{2\pi} d\varphi \int_0^{\ell'/2} \rho'(s')\, ds' = \frac{\text{area of}(\Sigma)}{(\lambda/2)^2}. \tag{26}$$

Because the tangential components over a surface enclosing the source determine the field everywhere, we conclude that the number of degrees of freedom of the field is essentially twice the number of sampling points, i.e., $2N$. This result has a very simple and appealing physical interpretation: the degrees of freedom of the fields radiated by *arbitrary* sources inside Σ are substantially coincident with those of an array of $\lambda/2$ spaced elements conforming to Σ. Leaving aside the relevance of this result in the areas of antenna synthesis, microwave diagnostics, and phase recovery, it is clear that a nonredundant field representation should use a number of parameters only slightly larger than that given by relation (26). As is shown in the next section with reference to ellipsoidal sources, sampling representations enjoy this property.

III. Spheroidal Sources

Let us now consider sources enclosed in a spheroid of rotation with major and minor semi-axes a and b, respectively. According to (19), the coordinate curves $\psi = \text{const}$ and $\xi = \text{const}$ through a point P in the meridian plane (x, z) bisect the angles formed by the tangents from P to $\mathcal{C}'$ (see Fig. 3). Now, in a centered conical section, the angles formed by the tangents from an external point and those formed by the straight lines from that point to the foci have the same bisectors. Because the bisectors of the lines from a point P to the foci coincide with the tangent and the normal to the confocal ellipse through P, we can conclude that the coordinate curves of the system (ψ, ξ) are the families of ellipses and hyperbolas confocal to $\mathcal{C}'$. This implies that ψ and ξ are functions only of the elliptic coordinates $v = (r_1 + r_2)/2a$[3] and $u = (r_1 - r_2)/2f$, respectively, $r_{1,2}$ being the distances from P to the foci and $2f$ the focal distance (see Fig. 3). In particular, ξ is equal to $\beta s'/W$, s' being the abscissa of the point P_0 wherein the

[3]With the choice $v = (r_1 + r_2)/2a$ instead of the more usual $v = (r_1 + r_2)/2f$, the equation of $\mathcal{C}'$ is $v = 1$ irrespective of its eccentricity.

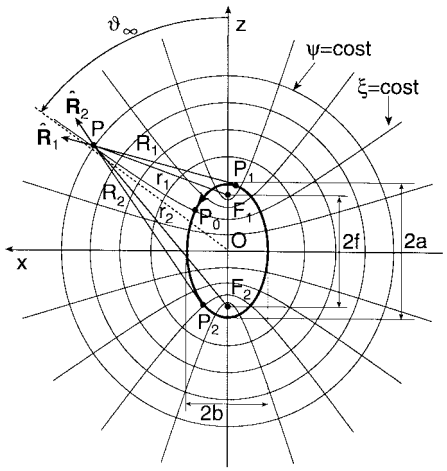

Fig. 3. The case of spheroidal sources.

hyperbola through P intersects $\mathcal{C}'$ (see Fig. 3) and ψ can be evaluated by considering a point on the symmetry axis. By lengthy but straightforward computations, with the choice $W = \beta\ell'/2\pi$ we get

$$\psi = \beta a\left[v\sqrt{\frac{v^2-1}{v^2-\varepsilon^2}} - E\left(\cos^{-1}\sqrt{\frac{1-\varepsilon^2}{v^2-\varepsilon^2}}|\varepsilon_2\right)\right] \tag{27}$$

$$\xi = \frac{\pi}{2}\cdot\begin{cases} E(\sin^{-1}u|\varepsilon^2)/E(\pi/2|\varepsilon^2)+1 & \text{prolate spheroid} \\ E(\sin^{-1}u|\varepsilon^2)/E(\pi/2|\varepsilon^2) & \text{oblate spheroid}\end{cases} \tag{28}$$

wherein $\varepsilon = f/a$ is the eccentricity of $\mathcal{C}'$ and $E(\cdot|\cdot)$ denotes the elliptic integral of second kind [5]. Note that the parameters u and v appearing in (27) and (28) have a simple geometrical meaning: (av) is the major semi-axis of the confocal ellipse through P, whereas

$$\sin^{-1}u = \begin{cases}\vartheta_\infty - \pi/2 & \text{prolate case} \\ \vartheta_\infty & \text{oblate case}\end{cases} \tag{29}$$

ϑ_∞ being the polar angle of the asymptote to the hyperbola through P (see Fig. 3). The choice of the pertinent branch of $\sin^{-1}$ is fixed by ϑ_∞.

Let us now consider the bandwidth W_φ relevant to an azimuthal circle intersecting the meridian plane at the point (ψ,ξ). Appendix B shows that W_φ is independent of ψ, i.e., the same bandwidth corresponds to all circles with the same value of ξ. Accordingly, $W_\varphi(\xi)$ can be evaluated by moving the circle to infinity along the hyperbola $\xi = \text{const}$; so taking (23) into account, we get

$$W_\varphi(\xi) = \begin{cases}\beta b\sin\vartheta_\infty(\xi) & \text{prolate case} \\ \beta a\sin\vartheta_\infty(\xi) & \text{oblate case}\end{cases} \tag{30}$$

wherein the asymptotic angle ϑ_∞ is obtained by inverting (28) and taking (29) into account.

Since W_φ depends only on ξ, the number of samples at the Nyquist rate over *any* rotational surface is constant and is given (for large sources) by relation (26). Accordingly, sampling representations over such surfaces are nonredundant.

The above results are now specified to the remarkable cases of "spherical" or planar sources. The first case can be handled by considering a spheroid with eccentricity $\varepsilon = 0$. Accordingly, the curves $\psi = \text{const}$ are circumferences, whereas the $\xi = \text{const}$ curves are radial lines. For an observation curve lying on a meridian plane we get $W = \beta\ell'/2\pi = \beta a$ and

$$\psi = \beta\sqrt{r^2-a^2} - \beta a\cos^{-1}(a/r) \tag{31}$$

$$\xi = \vartheta \tag{32}$$

since $v = r/a, \vartheta_\infty = \vartheta$ and $E(\vartheta|0) = \vartheta$ [5].

When the observation curve is an azimuthal circle, we get from (30)

$$W_\varphi = \beta a\sin\vartheta. \tag{33}$$

The case of a planar source, e.g., a disk $\mathcal{D}$ of radius a, can be treated as an oblate spheroid with eccentricty $\varepsilon \to 1$. With reference to an observation curve lying on a meridian plane we have $W = \beta\ell'/2\pi = 2\beta a/\pi$ and taking into account that [5]

$$E(\vartheta_\infty|1) = \int_0^{\vartheta_\infty}|\cos\tau|\,d\tau = \begin{cases}-2-\sin\vartheta_\infty & -3\pi/2 < \vartheta_\infty < -\pi/2 \\ \sin\vartheta_\infty & -\pi/2 < \vartheta_\infty < \pi/2 \\ 2-\sin\vartheta_\infty & \pi/2 < \vartheta_\infty < 3\pi/2\end{cases} \tag{34}$$

we get

$$\psi = \beta a(v-1) = \beta\left[\frac{r_1+r_2}{2} - a\right] \tag{35}$$

$$\xi = \frac{\pi}{2}\cdot\begin{cases}-2-u & \vartheta < -\pi/2 \\ u & -\pi/2 \le \vartheta \le \pi/2, \quad u = \dfrac{r_1-r_2}{2a} \\ 2-u & \vartheta > \pi/2.\end{cases} \tag{36}$$

For an azimuthal circle, we get directly from (21)

$$W_\varphi = \beta\left|\frac{r_1-r^2}{2}\right|. \tag{37}$$

Note explicitly that ξ is not analytic for $\vartheta = \pm\pi/2$. Accordingly (see Section II), the band-limitation error can be significantly higher near the equatorial plane, i.e., the plane containing the disk, than elsewhere. The same behavior is also expected in the case of very flat ellipsoids, wherein the singularities move outside the real axis of the complex ϑ plane, but are still very near to it. From the practical viewpoint, this drawback can be easily overcome when representing the field near the equatorial plane by considering the disk enclosed in a sphere of the same radius or in a confocal oblate spheroid and switching to the corresponding parameterization [see (31) and (32)].

IV. Application to Field Reconstruction

Previous results can be used to obtain fast and accurate sampling interpolation formulas from a nonredundant number of samples. While cardinal formulas could be used, central sampling series are more advisable from the point of view of numerical efficiency and make it possible to control error propagation from high- to low-level field regions [6], [7]. This requires a moderate increase of the sampling rate with respect

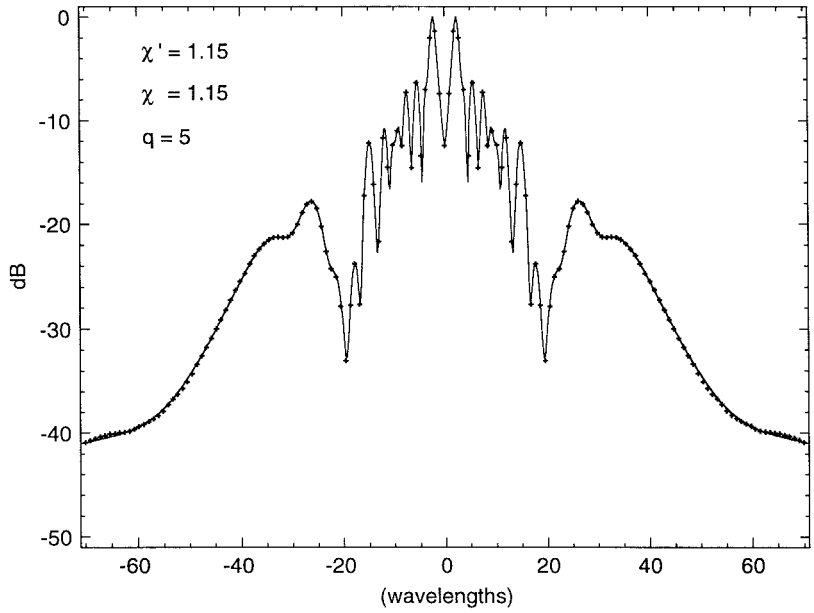

Fig. 4. Spherically modeled source. Amplitude of the field y component on the line $x = 0, z = 15\lambda$. Solid line: exact field; crosses: interpolated.

to the Nyquist rate corresponding to the adopted bandwidth $\chi' W$ being $\chi' > 1$ the factor that controls the band-limitation error.

The general expression of such a sampling representation over a generic curve is

$$\boldsymbol{F}(\xi) = \sum_{n=n_o-q+1}^{n_o+q} \boldsymbol{F}(\xi_n) D_M(\xi - \xi_n) \Omega_P(\xi - \xi_n) \qquad (38)$$

wherein $\xi_n = n\Delta\xi = 2\pi n/(2M+1), \chi > 1$ being the oversampling factor, $n_o = \mathrm{Int}(\xi/\Delta\xi)$[4] is the index of the sample closest to the output point, $2q$ is the number of retained samples and $M = \mathrm{Int}(\chi\chi' W)$.

In (38), $D_M(\cdot)$ denotes the Dirichlet polynomial of degree M

$$D_M(\xi) = \frac{\sin\left(\dfrac{2M+1}{2}\xi\right)}{(2M+1)\sin(\xi/2)} \qquad (39)$$

whereas $\Omega_P(\cdot)$ is an appropriate window function controlling the truncation error whose explicit expression is given in [6] and [7].

By applying (38) to meridian curves and azimuthal circles, nonredundant sampling expansions for various sources and observation geometries can be obtained [8]–[10].

In the following, two representative numerical tests are presented in order to validate the effectiveness of the proposed representations. In the first one, the source is considered as enclosed in a ball, i.e., (31) and (32) are used for ψ and ξ, while in the second one, the true source geometry is explicitly taken into account and, consequently, (35) and (36) are adopted. The examples are relevant to a nonfocusing planar circular array with diameter $2a = 24\lambda$ radiating a highly variable field to simulate severe reconstruction conditions. Its elements are elementary Huygens sources linearly polarized along the y axis, radially and azimuthally spaced by 0.6λ. Only 20% of them (randomly distributed) are active. Moreover, the array is symmetrical and symmetrically excited with respect to the x axis. The excitation amplitudes are tapered with respect to both the axes with a $\cos^2$ law and the phases are the superposition of a random term uniformly distributed in the range $(-\pi/2, \pi/2)$ and of a x-dependent cubic one.

With reference to the first example, Fig. 4 shows the reconstruction of the near-field y component (the most significant one) along the line $x = 0, z = 15\lambda$. The displayed y range subtends an angle equal to $2 \times 78° = 156°$. The overall number of employed samples (the $q = 5$ guard samples included) is 95, which is remarkably lower than the 305 required by applying the previous sampling representation [6].

To obtain a quantitative assessment of the algorithm performance, the maximum and mean-square reconstruction errors (normalized to the field maximum on this line) have been computed by comparing the reconstructed and the exact y component of the field, excluding the zone covered by the guard samples. Some values of the mean-square error are reported in Table I; the maximum error exhibits a quite similar behavior, being $\sim$10 dB higher. As can be seen, the attainable precision is very high in spite of the fact that $\gamma(\vartheta)$ is not analytic for $\vartheta = \pi/2$. This is obviously related to the behavior of the field, which goes to zero as ϑ approaches $\pi/2$.

Let us now consider the reconstruction of the field over a sphere by taking explicitly into account the true source geometry. Fig. 5 (dots) shows the near-field reconstruction along the H plane cut over a sphere of radius 25λ. As can be seen, notwithstanding the number of samples is halved with respect to a "spherical" modeling, the reconstruction is very good except for the neighborhood of $\vartheta = 90°$ wherein ξ is not regular. As stated in the previous section, we can obviate such an obstacle by adopting in this neighborhood the representation relevant to a spherical source. This is demonstrated in the same figure wherein triangles show the reconstruction obtained by

[4] $\mathrm{Int}(x)$ denotes the integer part of x.

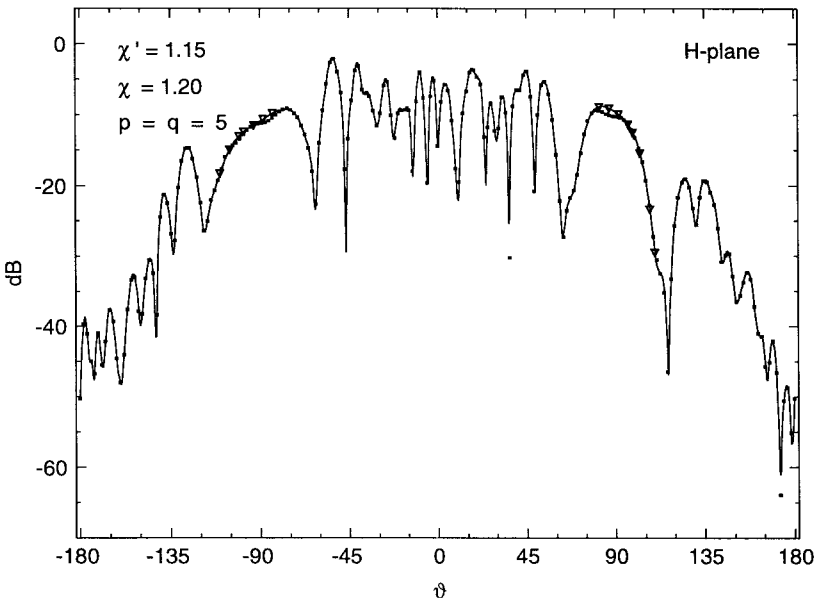

Fig. 5. Planar source. H plane cut over a sphere of radius 25λ. Solid line: exact field; dots: interpolated; triangles: interpolated from spherically modeled source.

TABLE I
MEAN-SQUARE RECONSTRUCTION ERROR (DECIBELS) ON THE LINE $x = 0, z = 15\lambda$

	χ=1.10	χ=1.15	χ=1.20	χ=1.25
p=q=3	-37.04	-40.14	-42.70	-45.22
p=q=5	-44.97	-50.77	-55.21	-59.33
p=q=7	-53.40	-62.03	-68.26	-73.69
p=q=9	-60.29	-71.66	-80.02	-87.20
p=q=11	-67.21	-80.95	-90.76	-96.61
p=q=13	-73.87	-89.77	-97.52	-98.83

switching to the "spherical" source in the interval [82°, 110°].

Finally, it must be stressed that an extensive numerical analysis has also assessed that, as expected, the above representations enjoy the same stability with respect to errors affecting the data as previously developed ones [7].

V. CONCLUSIONS

The problem of developing nonredundant representations of radiated or scattered EM fields over curves or surfaces has been thoroughly investigated and fully resolved. It has been shown that EM fields can be accurately represented by a finite number of samples, whatever the observation domain, even if unbounded. Such a number is essentially coincident with the number of degrees of freedom of the field, which is independent of the observation domain and depends only on the source geometry. Spheroidal sources have been analyzed in detail and the cases of spherical and discoidal sources have been explicitly dealt with.

Precise, fast, and stable sampling algorithms of central type have been applied to these source geometries on simple observation domains. The approach can be suitably extended to other observation domains and source geometries and can also be applied to the interpolation from power samples provided that the sample spacings are halved since, in this case, the bandwidth doubles.

It must be stressed that these results have a significant relevance in NF-FF transformation techniques and in other direct problems and become even more relevant in the "inverse problems" area where, due to the ill-posedness of the problem, it is mandatory to represent the EM field in a nonredundant way.

APPENDIX A
THE EQUIVALENT BANDWIDTH FOR AN AZIMUTHAL CIRCLE

Let us consider an azimuthal circle of radius ρ and center $(0, 0, z)$ (see Fig. 2). The Cartesian coordinates of a point P over this circle are $(\rho\cos\varphi, \rho\sin\varphi, z)$, whereas those of a point P' belonging to V are $(\rho'\cos\varphi', \rho'\sin\varphi', z')$. Because the phase factor and the local bandwidth are independent of the angle φ, we can assume, without any loss of generality, $\varphi = 0$. Accordingly

$$\left.\frac{\partial\gamma}{\partial\varphi}\right|_{\varphi=0} = -\beta\frac{\partial R}{\partial\varphi} = \frac{\beta\rho\rho'\sin\varphi'}{\sqrt{\rho^2+\rho'^2+(z-z')^2-2\rho'\rho\cos\varphi'}}. \tag{40}$$

As the extreme values of $\partial R/\partial\varphi$ are opposite and attained on Σ, we have from (9)

$$W_\varphi = \max_{\boldsymbol{r}'\in\Sigma}\left.\frac{\partial\gamma}{\partial\varphi}\right|_{\varphi=0} = \max_{z'}\left(\max_{\varphi'}\frac{\beta\rho\rho'\sin\varphi'}{\sqrt{\rho^2+\rho'^2+(z-z')^2-2\rho'\rho\cos\varphi'}}\right) \tag{41}$$

wherein $\rho' = \rho'(z')$ according to the equation of the surface Σ.

It can be verified that the maximum with respect to φ' is attained when (42), as shown at the top of the next page, and

$$\cos\varphi' = \cos\varphi'_M = \frac{[\rho^2+\rho'^2+(z-z')^2]-\sqrt{[\rho^2+\rho'^2+(z-z')^2]^2-4\rho^2\rho'^2}}{2\rho\rho'} \tag{42}$$

is given by

$$\dot{\gamma}_M = \max_{\varphi'}\left.\frac{\partial\gamma}{\partial\varphi}\right|_{\varphi=0} = \beta\sqrt{\rho\rho'\cos\varphi'_M}. \tag{43}$$

As

$$(R^{\pm})^2 = (z-z')^2+(\rho\pm\rho')^2 = (z-z')^2+\rho^2+\rho'^2\pm 2\rho\rho' \tag{44}$$

we get from (42) and (43) by straightforward passages

$$\dot{\gamma}_M = \frac{\beta}{2}(R^+ - R^-) = \frac{\beta}{2}\left(\sqrt{(z-z')^2+(\rho+\rho'(z'))^2}\right. - \left.\sqrt{(z-z')^2+(\rho-\rho'(z'))^2}\right). \tag{45}$$

By substituting into (41), we get (21).

Appendix B
Bandwidth Properties of Azimuthal Circles for Spheroidal Sources

Due to the rotational symmetry, the analysis is carried out with reference to the xz plane.

Let us focus on a given bandwidth W_φ and regard the source S as a sum of elementary disks having radius ρ' and abscissa z' (see Fig. 6). For each disk $D(z')$, let us consider the hyperbola $\beta(R^+-R^-)/2 = W_\varphi$, which exists if $\rho'(z') \geq W_\varphi/\beta$. As the disk varies along z', the hyperbolas relevant to the bandwidth W_φ describe a family with parameter z'. This family has an envelope τ, which divides the plane into two parts; we call the first one, containing the positive z axis, the *inner* zone and the second one we call the *outer* zone. By construction, for all points in the inner zone, we have $\beta(R^+-R^-)/2 < W_\varphi$, whereas for each point in the outer zone there exists a disk such that $\beta(R^+-R^-)/2 > W_\varphi$. Accordingly, from (21) we conclude that an azimuthal circumference, which intersects the xz plane in a point belonging to the inner zone, has a bandwidth less than W_φ, whereas a circumference, which passes through a point belonging to the outer zone, has a bandwidth greater than W_φ. Consequently, τ is the locus of the azimuthal circles with bandwidth W_φ.

As is well known, the envelope τ can be evaluated by eliminating the parameter z' between the equation of the hyperbola family and its derivative (with respect to z') equated to zero, i.e., by solving the following system:

$$\begin{aligned} F(x,z,z') &= \frac{x^2}{w^2} - \frac{(z-z')^2}{f^2(z')-w^2} - 1 = 0 \\ \frac{\partial F}{\partial z'} &= \frac{2(z-z')[f^2(z')-w^2]+(z-z')^2\partial f^2/\partial z'}{[f^2(z')-w^2]^2} \\ &= 0 \end{aligned} \tag{46}$$

where $w = W_\varphi/\beta$ and $x = f(z')$ is the equation of the curve $\mathcal{C}'$.

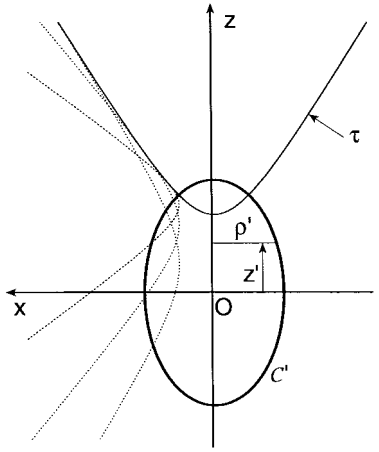

Fig. 6. Relevant to the bandwidth properties of azimuthal circles for spheroidal sources.

In the case of spheroidal sources, (46) can be easily solved and gives

$$\frac{z^2}{(a^2-b^2)(1-w^2/b^2)} - \frac{x^2}{(a^2-b^2)w^2/b^2} - 1 = 0 \tag{47}$$

for a prolate spheroid and

$$\frac{x^2}{(a^2-b^2)w^2/a^2} - \frac{z^2}{(a^2-b^2)(1-w^2/a^2)} - 1 = 0 \tag{48}$$

for an oblate one.

It can be easily recognized that (47) and (48) correspond to coordinate curves $\xi = \text{const}$. Accordingly, the azimuthal circles lying on the hyperbola $\xi = \text{const}$ have a constant bandwidth.

References

[1] O. M. Bucci and G. Franceschetti, "On the spatial bandwidth of scattered fields," *IEEE Trans. Antennas Propagat.*, vol. AP-35, pp. 1445–1455, Dec. 1987.

[2] O. M. Bucci and G. D'Elia, "Advanced sampling techniques in electromagnetics," in *Review of Radio Science 1993–1996*. London, U.K.: Oxford Univ. Press, 1996, pp. 177–204.

[3] O. M. Bucci and G. Franceschetti, "On the degrees of freedom of scattered fields," *IEEE Trans. Antennas Propagat.*, vol. 37, pp. 918–926, July 1989.

[4] O. M. Bucci and T. Isernia, "Degrees of scattered fields and attainable precision in electromagnetic inverse problems," in *Direct and Inverse Electromagnetic Scattering*. Reading, MA: Addison-Wesley, 1996, pp. 207–216 (Pitmam Res. Notes Math. Ser.).

[5] M. Abramowitz and I. Stegun, *Handbook of Mathematical Functions* New York: Dover, 1965.

[6] O. M. Bucci, C. Gennarelli, and C. Savarese, "Fast and accurate near-field far-field transformation by sampling interpolation of plane-polar measurements," *IEEE Trans. Antennas Propagat.*, vol. 39, pp. 48–55, Jan. 1991.

[7] ——, "Optimal interpolation of radiated fields over a sphere," *IEEE Trans. Antennas Propagat.*, vol. 39, pp. 1633–1643, Nov. 1991.

[8] O. M. Bucci, C. Gennarelli, G. Riccio, and C. Savarese, "Fast and accurate far-field evaluation from a nonredundant, finite number of

plane-polar measurements," in *Proc. IEEE-APS Int. Symp.*, Seattle, WA, June 1994, pp. 540–543.
[9] O. M. Bucci, C. Gennarelli, G. Riccio, C. Savarese, and V. Speranza, "Nonredundant representation of the electromagnetic fields over a cylinder with application to the near-field far-field transformation," *Electromagn.*, vol. 16, pp. 273–290, 1996.
[10] O. M. Bucci, C. Gennarelli, G. Riccio, and C. Savarese, "Near-field far-field transformation from nonredundant plane-polar data: Effective modelings of the source," *Proc. Inst. Elect. Eng. Microwaves, Antennas, Propagat.*, to be published.

Ovidio M. Bucci (SM'82–F'93), for photograph and biography, see p. 994 of the June 1997 issue of this TRANSACTIONS.

Claudio Gennarelli was born in Avellino, Italy, in 1953. He received the Laurea degree (*summa cum laude*) in electronic engineering from the University of Naples, Italy, in 1978.

From 1978 to 1983, he worked with the research group in electromagnetics at the Electronic Engineering Department of the University "Federico II," Naples. In 1983 he became a Research Engineer at the Istituto Universitario Navale, Naples. In 1987, as winner of a national competition, he was appointed an Associate Professor of Antennas at the Engineering Faculty of Ancona University, Ancona, Italy. He is currently an Associate Professor of Antennas at the Engineering Faculty of Salerno University, Italy. His main research interests are reflector antennas analysis, diffraction problems, radar cross-section evaluations, scattering from surface impedances, application of sampling techniques to electromagnetics, and to near-field far-field transformations.

Catello Savarese was born in Naples, Italy, in 1941. He received the Laurea degree (*summa cum laude*) in electronic engineering from the University of Naples, Italy, in 1967.

Since 1970, he has worked with the research group in electromagnetics in the Department of Electronic Engineering, University "Federico II," Naples, and at the Istituto Universitario Navale of Naples. In 1976 he was appointed an Assistant Professor of theory and techiques of eletromagnetic waves at the Istituto Universitario Navale of Naples and, in the same year, he became an Associate Professor of electromagnetics fields at the University "Federico II," Naples. Since 1986, as result of a national competition, he has been a Full Professor of antennas and radiowaves propagation at the Istituto Universitario Navale, Naples. His scientific interests include electromagnetic properties of material media, antennas in dispersive media, surface-impedance loaded-reflector antennas, microwave antennas analysis, representation of radiated electromagnetic fields, and near-field far-field transformation techniques.